MOLECULAR AND CELLULAR BIOLOGY, Mar. 2007, p. 2130–2143 Vol. 27, No. 6
0270-7306/07/$08.00+0 doi:10.1128/MCB.01826-06

A Triple Helix within a Pseudoknot Is a Conserved and Essential Element of Telomerase RNA▽

Kinneret Shefer,[1] Yogev Brown,[1] Valentin Gorkovoy,[1] Tamar Nussbaum,[1] Nikolai B. Ulyanov,[2]* and Yehuda Tzfati[1]*

Department of Genetics, The Silberman Institute of Life Sciences, The Hebrew University of Jerusalem, Givat Ram, 91904 Jerusalem, Israel,[1] *and Department of Pharmaceutical Chemistry, University of California at San Francisco, San Francisco, California 94158-2517*[2]

Received 26 September 2006/Returned for modification 9 November 2006/Accepted 19 December 2006

Telomerase copies a short template within its integral telomerase RNA onto eukaryotic chromosome ends, compensating for incomplete replication and degradation. Telomerase action extends the proliferative potential of cells, and thus it is implicated in cancer and aging. Nontemplate regions of telomerase RNA are also crucial for telomerase function. However, they are highly divergent in sequence among species, and their roles are largely unclear. Using in silico three-dimensional modeling, constrained by mutational analysis, we propose a three-dimensional model for a pseudoknot in telomerase RNA of the budding yeast *Kluyveromyces lactis*. Interestingly, this structure includes a U-A · U major-groove triple helix. We confirmed the triple-helix formation in vitro using oligoribonucleotides and showed that it is essential for telomerase function in vivo. While triplex-disrupting mutations abolished telomerase function, triple compensatory mutations that formed pH-dependent G-C · C^+ triples restored the pseudoknot structure in a pH-dependent manner and partly restored telomerase function in vivo. In addition, we identified a novel type of triple helix that is formed by G-C · U triples, which also partly restored the pseudoknot structure and function. We propose that this unusual structure, so far found only in telomerase RNA, provides an essential and conserved telomerase-specific function.

Telomerase, a ribonucleoprotein reverse transcriptase, makes up for losses caused by incomplete DNA replication and degradation, by adding species-specific, 5- to 26-nucleotide (nt) repeats onto the telomere termini (reviewed in reference 2). The telomerase complex contains an RNA subunit (TER) (TLC1 in *Saccharomyces cerevisiae*), a catalytic reverse transcriptase (TERT) (Est2 in *S. cerevisiae*), and several other protein components. Unlike other reverse transcriptases, telomerase specializes in repeatedly copying a short RNA template within its integral RNA component.

TERs are highly divergent, being conserved in sequence only among closely related species. Phylogenetic covariation was used to predict conserved secondary structures for evolutionarily close species of ciliates (14, 24), vertebrates (4), *Kluyveromyces* budding yeasts of the *K. marxianus* cluster (31, 32), and *Saccharomyces* sensu stricto (3, 7, 13, 37). Limited similarity in the general architecture was observed among these models, consisting of three long arms and a catalytic core domain (4, 13). Although nontemplate regions are essential for the assembly, regulation, and function of telomerase, their specific roles are still unclear (reviewed in reference 30). We hypothesized that important functional elements would exhibit better conservation in their tertiary structures, rather than in their secondary structures or sequences. Solving these tertiary structures may provide insights into their conserved functions.

Pseudoknot elements were found to be critical for telomerase function in ciliates (28), vertebrates (4), and *Kluyveromyces* (32). For *S. cerevisiae*, alternative pseudoknot models were suggested but experimental data failed to distinguish between them (3, 7, 10, 13). Interestingly, a TLC1 region, which includes the putative pseudoknot, is required for Est2 binding (3, 13, 15). However, the exact binding site is yet unknown.

To study the pseudoknot structure in detail, we introduced disruptive and compensatory mutations into the *Kluyveromyces lactis* TER gene (*TER1*), which were designed according to a preliminary secondary structure model (32). As described below, not all of the resulting phenotypes supported the model, suggesting the importance of tertiary interactions. These results guided us in three-dimensional (3D) modeling of the pseudoknot using the computer program miniCarlo (40). Interestingly, the modeling revealed a triple-helical stem within the pseudoknot as the only apparent structure consistent with the in vivo mutant phenotypes. We confirmed this prediction in vitro using short RNA constructs and showed by disrupting and compensatory mutations that the triple-helix formation is essential for the function of telomerase in vivo. A recently published nuclear magnetic resonance solution structure of the human telomerase pseudoknot revealed a similar triple-helix motif (29), making it the first structural motif conserved across the highly divergent yeast and vertebrate telomerase RNAs.

* Corresponding author. Mailing address for Nikolai B. Ulyanov: Department of Pharmaceutical Chemistry, University of California at San Francisco, San Francisco, CA 94158-2517. Phone: (415) 476-0707. Fax: (415) 502-8298. E-mail: ulyanov@picasso.ucsf.edu. Mailing address for Yehuda Tzfati: Department of Genetics, The Silberman Institute of Life Sciences, The Hebrew University of Jerusalem, Givat Ram, 91904 Jerusalem, Israel. Phone: 972-2-6584902. Fax: 972-2-6586975. E-mail: tzfati@cc.huji.ac.il.

▽ Published ahead of print on 8 January 2007.

MATERIALS AND METHODS

Yeast strains, genomic DNA preparation, and Southern hybridization. *K. lactis* deletion strain yJR27, based on the parental strain 7B520, was used for the CEN-ARS plasmid shuffling of wild-type (WT) and mutant TER genes as de-

scribed previously (25). Genomic DNA was prepared as described previously (18) except for omitting the proteinase K treatment. Southern analysis was performed as described previously (5). For BclI-specific hybridization, the 5′-end-^{32}P-labeled oligonucleotide KTElBcl (GATCAGGTATGTGG, where the underlined base is a locked nucleotide analog at the position corresponding to the BclI mutation) was used as a probe, hybridized at 40°C, and washed for 5 min with 0.2 M Na^+ twice at room temperature and once at 40°C. Hybridization with the WT telomeric probe (Klac1-25, ACGGATTTGATTAGGTATGTGGTGT) and the last wash were done at 50°C. Blots were exposed to film.

In vitro transcription of oligoribonucleotides. For radioactively labeled oligoribonucleotides, 80 pmol each of the T7 promoter oligonucleotide (common to all RNA constructs) and the specific CS3 or CS4 template oligonucleotide were incubated with 0.5 mM (each) CTP, ATP, and GTP; 0.1 mM UTP; [α-^{32}P]UTP (3,000 Ci/mmol; added amounts were calculated according to the number of uridines incorporated to yield equal specific activity for all RNA sequences), 1× transcription buffer (supplied by the manufacturer), and 20 units of T7 RNA polymerase (Ambion Inc.) in a 20-μl reaction mixture for 2 h at 37°C and then treated with 4 units of RNase-free DNase (Ambion Inc.) at 37°C for 15 min. Unlabeled RNA was transcribed with a MEGAshortscript T7 kit (Ambion Inc.) according to the manufacturer's instructions. The following T7 promoter (in lowercase) and WT template sequences were used; mutations were introduced to transcribe the mutant sequences described in Fig. 3A and B and 6A and B: T7 promoter oligonucleotide, taatacgactcactatagg; WT CS3, GGTTGGAAAAATC ACTAAAAAGAAAggtatagtgagtcgtatta; and WT CS4, TTGAGGTAAATGAT TTTATGggtatagtgagtcgtatta. All oligoribonucleotides were gel purified on a denaturing 8 M urea–15% polyacrylamide gel in 1× Tris-borate-EDTA; eluted from the gel slice twice in 300 μl of 0.5 M ammonium acetate, 1 mM EDTA, and 0.2% sodium dodecyl sulfate at 37°C for 2 h; precipitated with 5 μg glycogen, 0.3 M sodium acetate (pH 5.2), and 3 volumes of ethanol; resuspended in H_2O; and further purified with Microspin G-25 Sephadex columns (Amersham Biosciences).

Nondenaturing polyacrylamide gel electrophoresis. CS3 and/or CS4 oligoribonucleotides in the amounts indicated in the legends to Fig. 3 and 6 were heat denatured at 90°C for 2 min and cooled down at a rate of 1.7°C/min to 4°C in 44 mM sodium phosphate buffer (pH 6.25), 22 mM NaCl, and 5 mM $MgCl_2$ (for Fig. 3C) or in 10 mM MOPS (morpholinepropanesulfonic acid) buffer (pH 5 or 7 for Fig. 6C and D, respectively) and 5 mM $MgCl_2$. Then, 6% glycerol (for Fig. 3C) or 15% Ficoll (for Fig. 6C and D) was added, and samples were loaded onto nondenaturing polyacrylamide gels (15% or 10% acrylamide, respectively, and 1:40 bisacrylamide-acrylamide) in 6.7 mM Tris acetate, 3 mM sodium acetate, and 5 mM $MgCl_2$, (pH 6.25, 5, and 7 for the gels in Fig. 3C, 6C, and 6D, respectively). Gels were run at 4°C and 120 V for 18 h (for Fig. 3C), at 20°C and 250 V for 3 h (for Fig. 6C and D, right panels), or at 30°C and 250 V for 2 h (Fig. 6C and D, left panels). Results were visualized by autoradiography. Dried gels were exposed to a phosphorimager (Molecular Dynamics) or to film, and bands were quantified using the ImageJ program. The percentage of the dimeric form relative to the total (monomeric and dimeric) RNA was calculated.

Cloning and sequencing of telomeres. Individual telomeres were cloned by a ligation-mediated PCR method (31). The anchor oligonucleotide (CGTCGGC CGCGTCGTGACT) was phosphorylated at the 5′ end and had an inverted dT attached to the 3′ end by a 3′-3′ phosphodiester bond to allow ligation only to its phosphorylated 5′ end. The ligation reaction mixture (20 μl) contained 60 pmol anchor oligonucleotide, 0.5 μg genomic DNA, 50 mM Tris-HCl (pH 8), 10 mM $MgCl_2$, 1 mM dithiothreitol, 12.5% polyethylene glycol 8000, 1 mM hexamine cobalt chloride, 20 μM ATP (freshly added), 10 μg/ml bovine serum albumin, and 10 units RNA ligase (New England Biolabs) and was incubated for 90 min at 37°C. Ligated genomic DNA was purified by SureClean (Bioline Inc). Telomere fragments were amplified by PCR, using a subtelomeric primer (GACCG GGCCCAGCAGGACCAAG) present internally to 11 out of the 12 *K. lactis* telomeres and a primer complementary to the anchor oligonucleotides (AGTC ACGACGCGGCCGACG). PCR products were gel purified, digested with ApaI and EagI (introduced in the primers), cloned into a Bluescript SK vector, and sequenced with the M13 reverse primer (from the telomere end towards the subtelomere).

Thermal melting. RNA samples (1.0 to 2.0 μM each) were incubated in 10 mM MOPS buffer and 5 mM $MgCl_2$ at pH 5, 6, or 7. UV absorption (260 nm) was monitored with a UV spectrophotometer (Carry 300) attached to a temperature-controlled water circulator. The samples were incubated at 85°C for 2 min, and then the temperature was decreased to 20°C, paused at 20°C for 2 min, and then increased back to 85°C at a rate of 0.8°C/min with a 4-s data point averaging. Melting temperature (T_m) values were estimated from the graph of the first derivative of the curve of absorption versus temperature by using the computer program Origin.

Model building and molecular mechanic calculations. Model building and energy minimization of the pseudoknot structures were carried out with the miniCarlo program (40) on a cluster of Linux computers. The miniCarlo program performs molecular mechanic calculations of nucleic acid molecules, using internal coordinates as internal variables. The set of internal coordinates was designed specifically for nucleic acid structures, and it includes generalized helical parameters defining the relative positions of nucleic bases in space; aromatic bases are treated as rigid bodies with idealized geometry. The conformations of backbones connecting adjacent bases are calculated with a specialized chain closure algorithm (38), which ensures that bond lengths and bond angles have standard values. The conformational energy is calculated in vacuo with a distance-dependent dielectric constant, using an empirical force field optimized for nucleic acids (22, 39). To take the shielding effect of counterions into account, the phosphate groups are assumed to be electroneutral. Because of the simple geometric meaning of the independent variables, i.e., the helical parameters, the miniCarlo program can be used as a modeling tool with the help of the interactive molecular graphics program MIDASPlus (9) as described previously (33). Individual domains of the structure (such as stems or loops) were calculated with miniCarlo and then interactively arranged in space using MIDASPlus. After that, the internal coordinates defining the structure were calculated with Fitparam (34) and fed back to miniCarlo for the next iteration of energy optimization. Molecular graphics was prepared with MIDASPlus. The atomic coordinates of calculated models are available from the authors upon request.

RESULTS AND DISCUSSION

We previously identified a putative pseudoknot element in *K. lactis* telomerase RNA and showed that it is essential for telomerase function (32). The proposed structure was composed of two conserved sequences: CS3, forming stem 1 and a U-rich loop, and CS4, pairing with CS3 loop residues to form stem 2 (Fig. 1B). An unusual 3-nt bulge between stem 1 and stem 2 was expected to sharply distort the coaxial alignment of the two stems, which is normally observed in RNA pseudoknots (reviewed in reference 12). While the formation of stem 2 was validated experimentally (32), stem 1 has not been tested before and its formation was supported only by phylogenetic covariation among *Kluyveromyces* species (32). A similar pseudoknot was proposed for *S. cerevisiae* TLC1 (3, 7, 13). However, deleting the corresponding stem 1 had no apparent effect on telomere length in *S. cerevisiae* (3, 13). To analyze the pseudoknot structure in more detail, we designed mutations that disrupted, restored, or paired the predicted stems and single-stranded regions. We replaced the WT *TER1* gene in *K. lactis* with mutant genes by using a plasmid-shuffling system described previously (25) and tested the effects on telomerase activity in vivo. An additional single-nucleotide mutation was introduced into the TER template, resulting in the incorporation of BclI restriction sites into the telomeric repeats. Otherwise, this mutation is apparently silent and thus can be used to mark the nascent repeats incorporated by the investigated telomerase and reveal its in vivo activity (25). BclI repeats are identified by Southern analysis of telomeric fragments hybridized to a BclI-specific telomeric probe (Fig. 1A and D), or by BclI restriction endonuclease digestion and hybridization to a WT probe (Fig. 1A and E). The overall telomere length is revealed by the WT hybridization to telomeric fragments undigested with BclI (Fig. 1E). In yeast, a delicate balance between positive and negative regulation of telomerase activity maintains telomeres at a constant length. A change of less than 50% in the amount or activity of telomerase can impair the balance and affect telomere length (20). Therefore, telomere length can be used as a sensitive in vivo assay for telomerase activity. The results are described below.

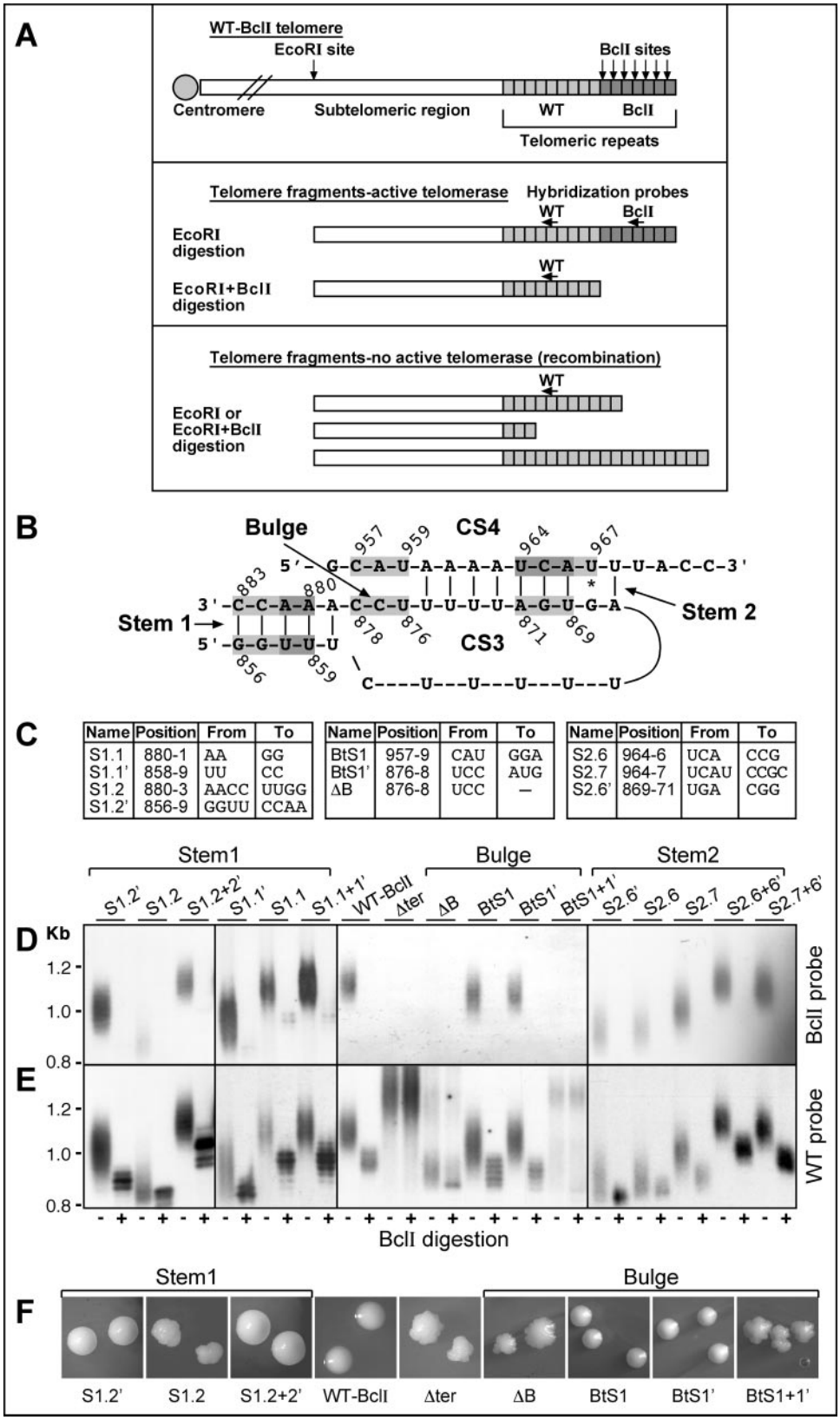

FIG. 1. Mutational analysis of the pseudoknot element. (A) Schematic representation showing telomeric fragments digested with restriction endonucleases EcoRI or EcoRI plus BclI and hybridization probes (WT and BclI specific). (B and C) Secondary structure model of the *K. lactis* pseudoknot element (B), with the positions of the mutations introduced to test stem 1, bulge, and stem 2 (C) highlighted in gray. (D and E) Plasmids carrying *ter1* genes with the template BclI mutation alone (WT-BclI), additional pseudoknot mutations, or an empty vector (Δ*ter*), as

TABLE 1. Summary of mutations and their effect on telomere function in vivo

Element	Name	Position	Sequence (5′ to 3′)		Colony phenotype[a]	Telomere length (% of WT)
			WT	Mutation		
Stem 1	S1.1	880–881	AA	GG	1	100
	S1.1′	858–859	UU	CC	2	50
	S1.1+1′				1	100
	S1.2	880–883	AACC	UUGG	3	30
	S1.2′	856–859	GGUU	CCAA	1–2	63
	S1.2+2′				1	94
Bulge	BtS1	957–959	CAU	GGA	1	90
	BtS1′	876–878	UCC	AUG	1	90
	BtS1+1′				4	Rec[b]
	ΔB	876–878	UCC	DEL	4	Rec
	BtS2	958	A	G	1	90
	BtS2′	876–878	UCC	GCG	1	90
	BtS2+2′				1	85
Stem 2	S2.0	960–962	AAA	GGG	4	30
	S2.0′	873–875	UUU	CCC	4	40
	S2.1	964–966	UCA	AGU		30–40
	S2.1′	869–871	UGA	ACU		30–40
	S2.2	961–963	AAA	UUU		Rec
	S2.2′	872–874	UUU	AAA		Rec
	S2.3	961–963	AAA	GGG		Rec
	S2.3′	872–874	UUU	CCC		Rec
	S2.4	961–963	AAA	CCC		Rec
	S2.4′	872–874	UUU	GGG		Rec
	S2.5	961–966	AAAUCA	GGGAGU		Rec
	S2.5′	869–874	UGAUUU	ACUCCC		Rec
	S2.5+5′					60
	S2.6	964–966	UCA	CCG		50
	S2.7	964–967	UCAU	CCGC		70
	S2.6′	869–871	UGA	CGG		50
	S2.6+6′				1	100
	S2.7+6′				1	90
Loop	L.a	862–864	UUU	CCC		
	L.b	863–865	UUU	CCC	3	Rec
	L.c	864–866	UUU	CCC	3–4	Rec
	L.d	864–866	UUU	AAA	3–4	Rec
	L.e	866	U	C	1	100
Other	S2.0′+L.b				4	Rec
	S2.0′+L.a				4	Rec
	S2.3′+L.c				4	Rec
	S2.3+L.c				4	Rec

[a] Colony phenotypes are rated according to the severity of the phenotype from 1 (the smooth appearance of wild-type strains) to 4 (the severe, rough phenotype observed in a *ter*Δ strain).

[b] Rec, deregulated telomere length typical of the alternative, telomerase-independent recombination pathway. Such a phenotype is observed in a *ter*Δ strain after its telomeres shorten to a critical length.

Stem 1. Two sets of mutations were designed to test stem 1. Each set consisted of two disrupting mutations in either strand of stem 1 and a double mutation (the combination of the two) predicted to restore the base pairing (Fig. 1B and C). One set was composed of 2-nt mutations (S1.1, S1.1′, and S1.1+1′) and another set of 4-nt mutations (S1.2, S1.2′, and S1.2+2′). Out of four single mutations, S1.1′ and S1.2 caused severe telomere shortening and a rough colony phenotype, a hallmark of impaired telomere maintenance in *K. lactis* (Fig. 1D, E, and F and Table 1). S1.2′ caused moderate telomere shortening, which did not affect the colony phenotype. In the fourth mutation, S1.1, two guanines were substituted for adenines and could

indicated above the lanes (D), were used to replace the WT *TER1* gene encoded on a URA plasmid. Genomic DNA was prepared from the resulting *K. lactis* strains in their sixth passage and analyzed by a Southern blot hybridized first with a BclI-specific (D) and then with a WT (E) probe. Only portions of the gel are shown, which include a group of 7 out of the 12 *K. lactis* telomeres. (F) Typical colony phenotypes of *K. lactis* strains taken at their fourth passage. Impaired telomere maintenance is associated with rough colony appearance, as opposed to the smooth WT colonies.

TABLE 2. Characterization of double and triple mutants of stem 2

Pseudoknot mutation	Colony phenotype[a]	TER level[b] (% of WT)	Telomere length (% of WT)	T_m (°C)[d] at pH:			Dimer formation (% of total signal)[e] at:				
							4°C, pH 6.25	20°C		30°C	
				5	6	7		pH 5	pH 7	pH 5	pH 7
WT	1	100	100	54.5	55	50	+	100	100	100	100
S2.0+0′	2–3		50	55	55	55		49	40	52	28
S2.1+1′	1		100				+				
S2.2+2′	3–4		Rec–40[c]				−				
S2.3+3′	1–2	80	60–80	57	57	56	−/+	53	27	37	14
S2.4+4′	3		40								
S2.0+0′+L.a	4		30								
S2.0+0′+L.b	1–2		65	65	55	55		100	57	100	42
S2.2+2′+L.d	4		Rec								
S2.3+3′+L.b	4	57	Rec					66	43	56	37
S2.3+3′+L.c	1–2	82	60–80	71	63	55	+	100	51		38

[a] Colony phenotypes are rated according to the severity of the phenotype from 1 (the smooth appearance of WT strains) to 4 (the severe, rough phenotype observed in a *ter*Δ strain).
[b] TER levels were measured by Northern analysis, quantified with a phosphorimager, and corrected to the signal measured for 18S rRNA, as described previously (32).
[c] Rec, deregulated telomere length typical of the alternative, telomerase-independent recombination pathway. Such a phenotype is observed in a *ter*Δ strain after its telomeres shorten to a critical length. Rec–40 indicates variability among different clones. Some clones show short but stable telomeres (40% of the WT length), and some reveal deregulated telomere length typical of the recombination pathway.
[d] Determined by UV melting experiments.
[e] Determined by nondenaturing PAGE. Indicated are the portions (percentage) of the dimer form out of the total radioactive signal. +, formation of dimers; −, no dimer formation; −/+, partial dimer formation.

potentially form wobble pairs with their uridine counterparts. As expected, this mutation did not affect telomere length and colony phenotype. It is not clear why the severity of the disrupting mutation S1.2 was different from that of S1.2′. It is possible that the more severe effects of S1.1′ and S1.2 reflect tertiary interactions impaired by these mutations. Alternatively, new interactions may form by the mutated sequences, which are more detrimental for the pseudoknot structure and function than the destabilization of stem 1 by S1.2′. However, it is important that the compensatory mutations fully restored normal telomere length and colony phenotype, confirming that the formation of stem 1 is important for telomerase function in vivo.

The bulge. Normally, the two stems of a pseudoknot are stacked in a continuous helix. A bulge of 1 to 2 nt between the stems would introduce a kink in the helix, which may have biological implications (12). A preliminary 3D model (not shown) predicted that a 3-nt bulge between the two stems in the *K. lactis* pseudoknot, as appears in the secondary structure model (Fig. 1B), would introduce a sharp kink in the structure. To test the conformation and importance of the bulged nucleotides, we designed mutations to eliminate the bulged nucleotides or to pair them with CS4 residues (Fig. 1B and C). Deleting the 3-nt predicted bulge completely abolished telomerase activity, as revealed by the lack of BclI repeat incorporation (Fig. 1D), the deregulated telomere length (Fig. 1E, compare ΔB to Δ*ter*) typical of the telomerase-independent alternative pathway for telomere maintenance (17), and the rough colony phenotype (Fig. 1F). Surprisingly however, 3-nt substitutions in either CS3 or CS4, designed to pair the bulged nucleotides and eliminate the putative kink in the structure, only slightly reduced telomere length and did not affect colony phenotype (Fig. 1D, E, and F, BtS1 and BtS1′). In contrast, the double mutation composed of BtS1 and BtS1′ together abolished telomerase function in vivo (Fig. 1D, E, and F, BtS1+1′). These results suggested that the nucleotides previously thought to form a bulge might actually be paired, enabling the coaxial alignment of the two stems. Therefore, the BtS1 and BtS1′ mutants, which maintained base-pairing, did not significantly affect the structure. In the double mutant BtS1+1′, the substituted $AUG_{876–878}$ nucleotides of BtS1′ may interact with the $CUU_{861–863}$ of the CS3 loop, effectively extending stem 1 instead of stem 2. This change abolished telomerase function, indicating that the junction between the two stems and possibly the CS3 loop nucleotides are critical. The possibility of the two stems stacked into a continuous helix was puzzling—how could a pseudoknot structure accommodate a 10- to 12-nt-long stem 2 (a full helical turn of an A-form double helix) connected at both ends by a short 6-nt loop (Fig. 1B)? This puzzle inspired further research as described below.

Stem 2. Mutations in one part of stem 2 ($UCA_{964–966} \cdot UGA_{869–871}$) (Fig. 1B and C), designed to disrupt stem 2, caused severe telomere shortening. Compensatory mutations, designed to restore this part of stem 2 with altered sequences, fully restored telomerase function and normal telomere length, consistent with the pseudoknot model (S2.6, S2.6′, and S2.6+6′ in Fig. 1; S2.1, S2.1′, and S2.1+1′ in reference 32; and Tables 1 and 2). Similar results were obtained for the corresponding part of stem 2 in *S. cerevisiae* TLC1 (see mutants *tlc1-29*, *tlc1-30*, and *tlc1-31* in reference 3 and no. 20, 21, and 22 in reference 13).

Interestingly, S2.7 telomeres were not as short as S2.6 telomeres (Fig. 1D and E). Since the only difference between the two mutations is an additional change of U_{967} to C in S2.7, this observation suggested that C_{967} is paired with G_{868} in the S2.7 mutant, partially compensating for the disruption of two A · U pairs. Altogether, these observations suggested that in the S2.7 and S2.7+6′ mutants, and possibly also in the WT, G_{868} is paired, implying that stem 2 may span over 12 bp (including the last $A_{867}U_{968}$ pair).

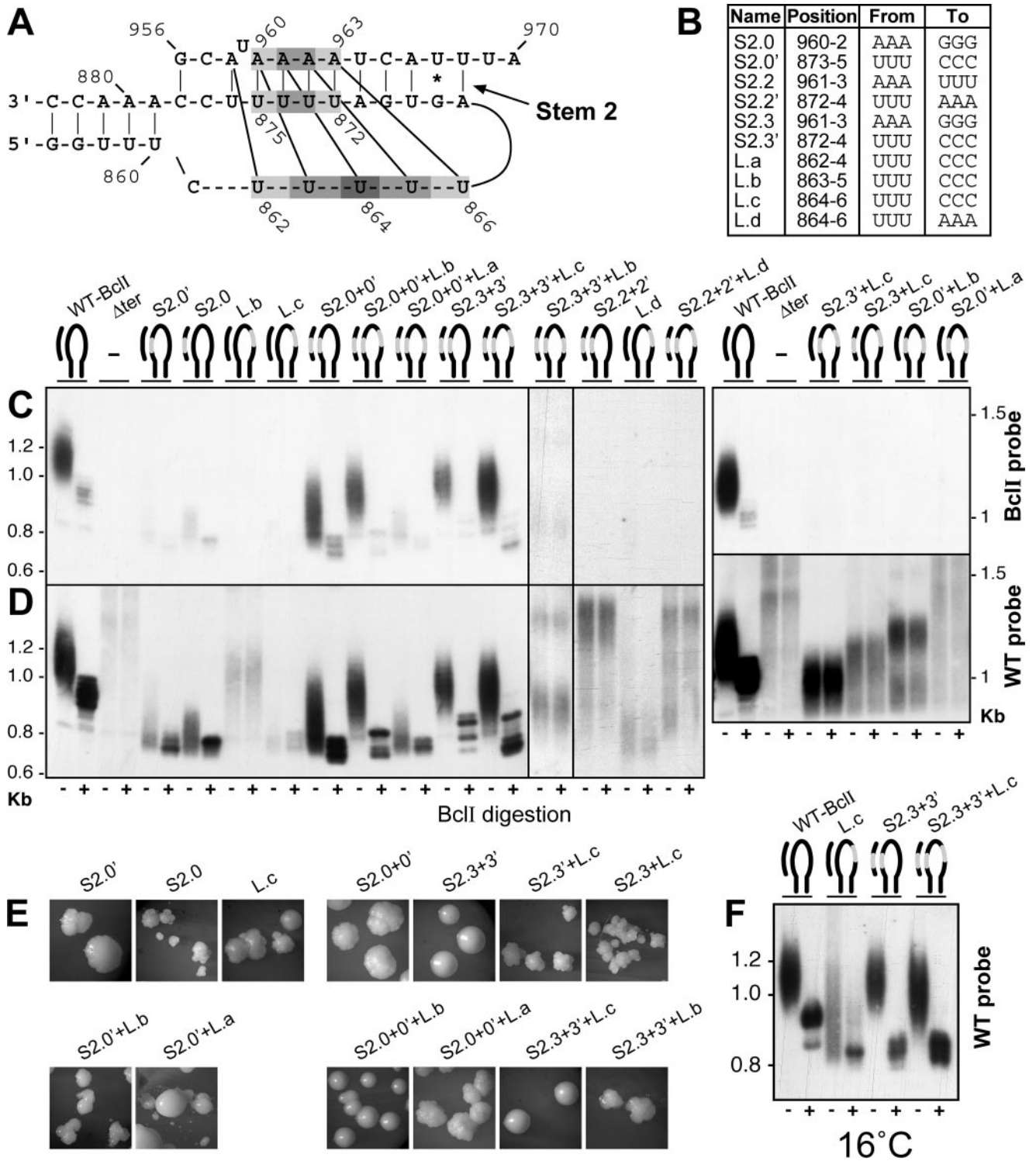

FIG. 2. Mutational analysis of the triple-helical stem. (A) Secondary structure model of the *K. lactis* pseudoknot element. Highlighted in gray are the positions of the mutations introduced into the *TER1* gene to test the triple-helical stem. (B and C) The mutations are described (B) and indicated in gray on the small schematic representations of the pseudoknot above the lanes in panel C. (C and D) Genomic DNA was prepared from the various *K. lactis* strains in their sixth passage and analyzed with a Southern blot hybridized with Bcl-specific (C) and WT (D) probes, as described for Fig. 1. (E) Typical colony phenotypes of the strains at their fourth passage. (F) WT hybridization to telomere fragments of strains grown at 16°C (for six passages on plates and then in liquid medium) instead of at the normal temperature of 28 to 30°C.

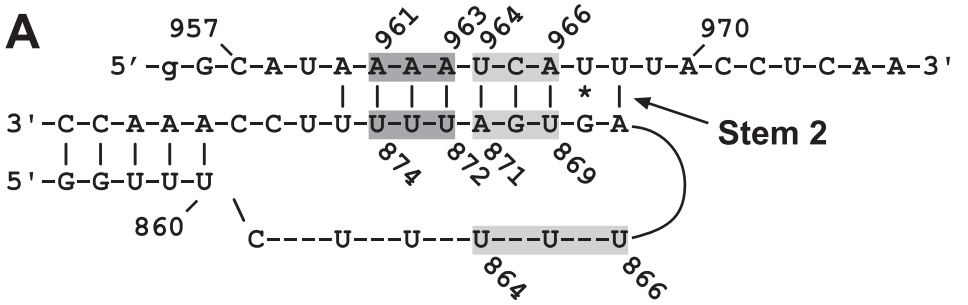

B

Name	Position	From	To
S2.1	964-6	UCA	AGU
S2.1′	869-71	UGA	ACU
S2.2	961-3	AAA	UUU
S2.2′	872-4	UUU	AAA
S2.3	961-3	AAA	GGG
S2.3′	872-4	UUU	CCC
L.c	864-6	UUU	CCC

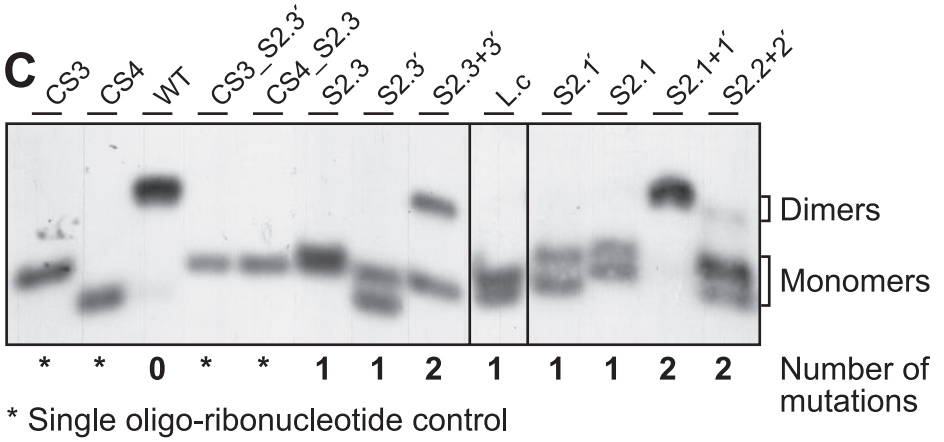

FIG. 3. Dimer formation by oligoribonucleotides. (A and B) Secondary structure model of the *K. lactis* pseudoknot element (A), with the positions of the mutations introduced to test stem 2 and the CS3 loop (B) highlighted in gray. The first G residue in CS4 (in lowercase) is not present in the WT sequence but was introduced to facilitate efficient transcription by T7 RNA polymerase. (C) The WT and mutated CS3 and CS4 oligoribonucleotides (0.01 pmol each) described in panels A and B, both radioactively labeled, were denatured, renatured, and analyzed by 15% nondenaturing PAGE at 4°C and pH 6.25. Single oligoribonucleotides are indicated by CS3 or CS4 and asterisks below the lanes. Lanes with mixtures of both CS3 and CS4 are labeled by the name (above) and number (below) of the mutations introduced. Note that the mutant CS4-S2.3 oligoribonucleotide migrated slower than the WT CS4, presumably because the mutated (but not the WT) CS4 alone can form a stable dimer. Since it comigrated with the longer CS3, only one band corresponding to the monomer form appears under S2.3 and S2.3+3′.

When the other part of stem 2 ($AAAA_{960–963} \cdot UUUU_{872–875}$) (Fig. 1B) was tested, again single mutations in either strand severely disrupted or completely abolished telomerase function (S2.0 and S2.0′ in Fig. 2; S2.2, S2.2′, S2.3, S2.3′, S2.4, and S2.4′ in reference 32; and Table 1). However, in contrast to the first part of stem 2, in this part the double compensatory mutations did not restore at all or only partially restored normal telomere length (S2.0+0′, S2.2+2′, S2.3+3′, and S2.4+4′ in Fig. 2; Table 2) (32). Interestingly, a stretch of three to five A · U base pairs is conserved in this part of stem 2 in the predicted pseudoknots of *Kluyveromyces*, *Saccharomyces*, and vertebrate TERs. Similar results were obtained with *S. cerevisiae* for this corresponding part of stem 2 (mutations 17, 18, and 19 in reference 13 and *tlc1-43*, *tlc1-44*, and *tlc1-45* in reference 3). We next asked whether the inability of double mutations in the $AAAA_{960–963} \cdot UUUU_{872–875}$ part of stem 2 to restore normal telomerase function was caused by impaired CS3-CS4 interaction or by additional, unknown RNA-RNA or protein-RNA interactions. We synthesized short oligoribonucleotides composed of WT and mutated CS3 (28-nt) and CS4 (22-nt) sequences and analyzed their interaction by native polyacrylamide gel electrophoresis (PAGE) (Fig. 3). WT CS3 and CS4 together formed low-mobility bands, presumably corresponding to CS3-CS4 dimers (Fig. 3C, WT). Dimer formation was dependent upon Mg^{2+} ions (not shown). Incorporating 3-nt mutations designed to disrupt stem 2 (S2.1, S2.1′, S2.3, and S2.3′), abolished dimer formation. As expected, the double compensatory mutation S2.1+1′ fully restored dimer formation. Strikingly however, the double mutation S2.3+3′ in the $AAAA_{960–963} \cdot UUUU_{872–875}$ part of stem 2 only partially restored dimer formation, despite the expected stabilizing effect of replacing three A · U with three G · C base pairs. Double transversion mutations at these positions, introducing three U · A pairs (S2.2+2′) or three C · G pairs (S2.4+4′) (not shown) almost completely abolished dimer formation. Furthermore, a 3-nt mutation (L.c) in the loop region of CS3 also completely abolished dimer formation, although the residues predicted to form stem 2 were unchanged. These results suggested that tertiary interactions were required to stabilize the dimer formation. Such interactions may have been weakened by the double mutation S2.3+3′ and completely disrupted by the double mutations S2.2+2′ and S2.4+4′ and by the loop mutation L.c. Importantly, the formation of stable dimers in vitro correlated well with the ability of the corresponding sequences to support telomerase function in vivo: the S2.3+3′ mutant had a moderate effect on telomerase function, while the S2.2+2′,

S2.4+4′, and L.c mutants completely abolished or severely impaired telomerase function (Fig. 2; Tables 1 and 2) (32).

Altogether, the conservation of primary sequence among species, the inability of compensatory mutations to fully restore dimer formation in vitro and telomerase function in vivo, and the effect of mutations in the CS3 loop suggested that the $AAAA_{960–963} \cdot UUUU_{872–875}$ part of stem 2 and the CS3 U-rich loop are involved in non-Watson-Crick tertiary interactions essential for the formation of a stable pseudoknot structure.

Modeling a pseudoknot with a triple-helical stem. We checked the feasibility of forming a pseudoknot structure by CS3 (nt 856 to 883) and CS4 (nt 960 to 968), i.e., whether the sizes of stem 1 (nt 856 to 860 and 879 to 883), stem 2 (nt 867 to 875 and 960 to 968), and the loop (nt 861 to 866) are compatible with a pseudoknot architecture. At first we assumed that the UCC linker (nt 876 to 878) between the two stems remained single stranded. The critical question was whether the length of the loop, 6 nt, would be sufficient to span the length of stem 2 (initially assumed to be 9 bp), connecting the ends of stem 1 (nt 860) and stem 2 (nt 867). Modeling with the miniCarlo program showed that the length of the loop was indeed more than sufficient to fit into a pseudoknot structure (not shown). As is common for pseudoknots with two coaxial stems (36), the loop crossed the major groove of stem 2. It was located outside of the groove and had an irregular conformation.

However, as described above, mutational analysis suggested that the $UCC_{876–878}$ sequence, previously thought to be single stranded, is actually paired. First attempts to model the stem extension mutants (BtS1 and Bts2+2′) (see Table 1) showed that the loop (nt 861 to 866) became very strained and started to penetrate the major groove of stem 2, which caused multiple interatomic clashes (not shown). It became obvious that for this mutant sequence to form a pseudoknot, the loop must be located inside the major groove of stem 2. A possible way to prevent interatomic clashes and stabilize this structure is to form a triple-helical stem. Although such a major-groove triple helix was first discovered for synthetic RNA in 1957 (8), high-resolution structures were available only for DNA. Therefore, we modeled a regular poly(rU)-poly(rA) · poly(rU) triple helix using miniCarlo (Fig. 4A). As in DNA triple helices (11), bases from a poly(rU) strand and a poly(rA) strand form Watson-Crick pairs, while the third strand, poly(rU), is located in the major groove in an orientation parallel to the poly(rA) strand, and its bases form Hoogsteen-type hydrogen bonds with the adenines (Fig. 4C). The backbones of all three strands have conformations typical of the A-family of forms, including the C3′-*endo* sugar puckers. The duplex formed by the Watson-Crick strands has a major groove somewhat wider than a typical duplex A-RNA, to accommodate the third strand. One distinction of the RNA triple helix from its DNA counterpart is an additional hydrogen bond between the hydroxyl group of each uridine of the third strand and the phosphate oxygen of the poly(rA) strand. This hydrogen bond is relatively weak, with a proton-to-oxygen distance of 2.4 Å, but it is nevertheless a stabilizing interaction. Using this triple helix, we built and refined the model for the stem extension BtS1 mutant (not shown). It has five consecutive U-A · U triples, U_{876}-$a_{959} \cdot U_{862}$, U_{875}-$A_{960} \cdot U_{863}$, U_{874}-$A_{961} \cdot U_{864}$, U_{873}-$A_{962} \cdot U_{865}$, and U_{872}-$A_{963} \cdot U_{866}$, incorporated in stem 2

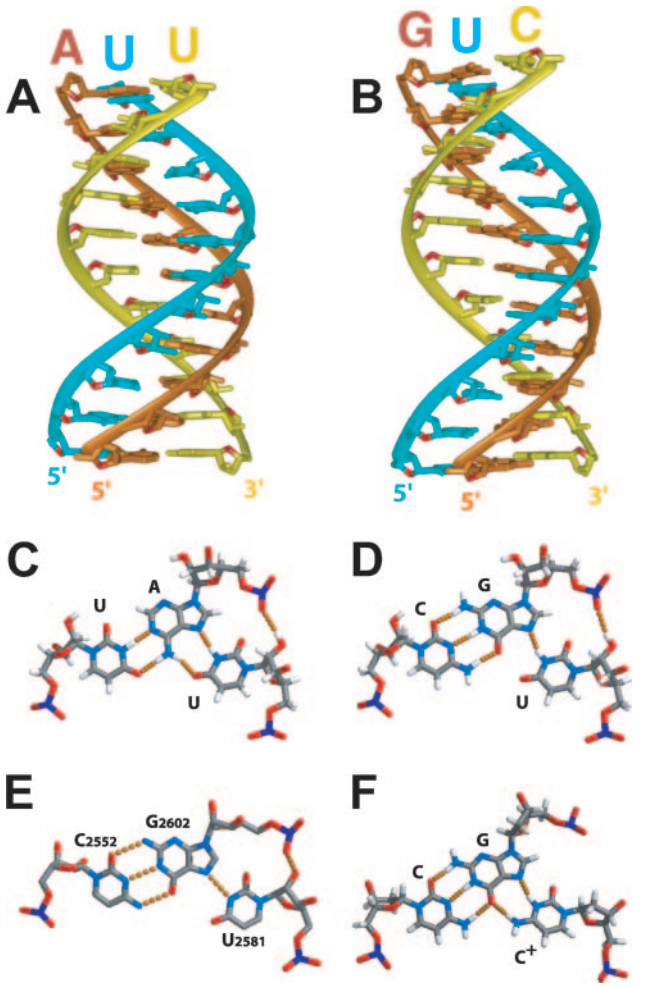

FIG. 4. Triple-helix models. Modeling was performed using miniCarlo as described in Materials and Methods. (A and B) Eleven triples are shown for poly(rU)-poly(rA) · poly(rU) (A) and poly(rC)-poly(rG) · poly(rU) (B). In each strand, conformations of consecutive residues are identical. Watson-Crick strands are colored in brown (purine strand) and yellow (pyrimidine strand), and the third poly(rU) strand is colored in cyan. Backbones are schematically shown as ribbons, and sugar O4′ atoms are colored in red. (C) A typical U-A · U triple from the WT pseudoknot model. (D) A C-G · U base triple from the model of the pseudoknot structure for the S2.3+3′ mutant. (E) An example of a single C-G · U base triple found in the crystal structure of the *Haloarcola marismortui* 50S ribosomal subunit (1). (F) An example of a C-G · C^+ base triple from a DNA triplex (PDB 149D) (23).

(lower case indicates a mutated residue). C_{877} forms a Watson-Crick pair with g_{958} and C_{878} with g_{957}. If protonated, C_{861} has a potential to form an additional base triple, C_{877}-$g_{958} \cdot C_{861}^{+}$. Importantly, there are no interatomic clashes in this model.

The model for the pseudoknot structure of the WT *K. lactis* sequence (Fig. 5A) was calculated in a similar way. Stem 2 is divided into two segments: the lower part consists of five U-A · U base triples, U_{876}-$A_{958} \cdot U_{862}$, U_{875}-$A_{960} \cdot U_{863}$, U_{874}-$A_{961} \cdot U_{864}$, U_{873}-$A_{962} \cdot U_{865}$, and U_{872}-$A_{963} \cdot U_{866}$, and the upper part consists of five base pairs, including four Watson-Crick pairs and the wobble G_{868}-U_{967} pair (Fig. 5B). Residues C_{861}, C_{877}, and C_{957} are unpaired in this model. They are located inside stem 2 between the last triple (U_{876}-$A_{958} \cdot U_{862}$)

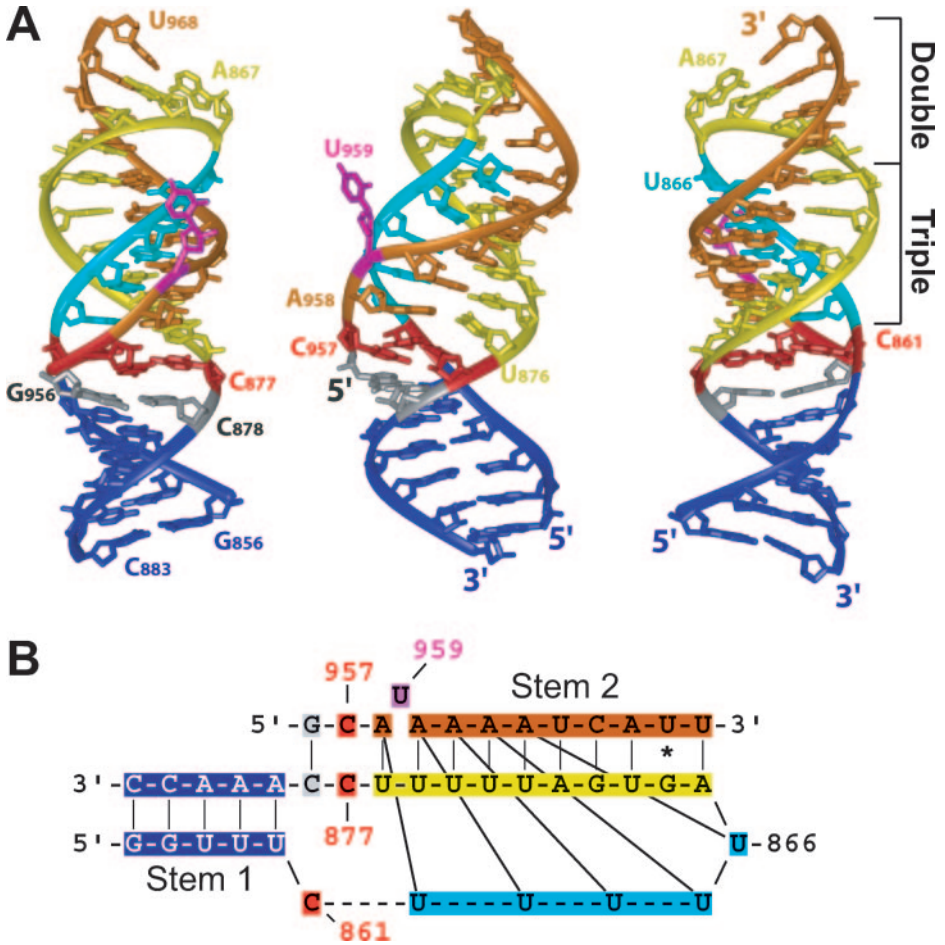

FIG. 5. A three-dimensional model for the wild-type pseudoknot structure. Modeling was performed using miniCarlo as described in Materials and Methods. (A) A ribbon representation (three different views). Stem 1 is shown in blue, Watson-Crick strands of stem 2 are colored in brown (purine-rich strand) and yellow (pyrimidine-rich strand), and the third oligo(U) strand is colored in cyan. Bulged-out U_{959} is shown in magenta; unpaired residues C_{861}, C_{877}, and C_{957} underneath the last triple are in red; and the Watson-Crick pair C_{878}-G_{956} terminating stem 2 are in gray. (B) A schematic representation of base-pairing in the pseudoknot. Vertical lines represent Watson-Crick interactions; tilted lines, Hoogsteen interactions; and the asterisk, a G · U wobble pair. Note that if protonated, C_{861} has a potential to form a base triple (C_{878}-G_{956} · C_{861}^{+}).

and the terminal Watson-Crick pair (C_{878}-G_{956}), but their precise conformation cannot be predicted with certainty and may be quite flexible. Interestingly, these three unpaired cytosines are not conserved in the *Kluyveromyces* sequences (see Fig. 8). Residue U_{959} is bulged out between two base triples in the model. It is conserved in four out of six *Kluyveromyces* sequences.

Additional modeling calculations showed that a slightly different pseudoknot conformation with a comparable energy is also possible for the WT sequence. In this conformation, the register of the third strand is shifted by one position relative to the duplex, forming only four U-A · U triples and affecting mostly the conformation of the junction between the two stems (not shown).

One more modeling experiment was carried out to explain the moderate effect of the double transition mutation S2.3+3′ on dimer formation in vitro and on telomerase function in vivo, compared to the severe effects of the double-transversion mutations S2.2+2′ and S2.4+4′ (Fig. 2; Table 2) (32). Formation of a structure similar to that of the WT by the S2.3+3′ mutant would require the formation of C-G · U triples in the triple-helical part of stem 2. To the best of our knowledge, such triplexes have not yet been described in the literature. Surprisingly, computer modeling showed that a perfect triple helix can be formed by C-G · U triples, almost identical in conformation to the U-A · U triple helix (Fig. 4B). The H3 atom of the uracil from the third strand forms a single hydrogen bond with the guanine N7, and there is an additional weak hydrogen bond between the uridine hydroxyl group and the phosphate oxygen of the guanine (Fig. 4D). The electronegative atom O4 of the uracil is juxtaposed against the electronegative atom O6 of the guanine with a relatively short distance of 2.9 Å, resulting in a slight increase in the conformational energy. However, this increase was compensated for by other interactions in the triple helix. We found a similar single base triple (Fig. 4E) in the crystal structure of the *Haloarcola marismortui* 50S ribosomal subunit (1). In the ribosomal structure, this triple is isolated and unconstrained by the overall geometry of a triple helix. Thus, O4 and O6 are positioned at a more optimal distance of 4.0 Å. The high similarity between the conforma-

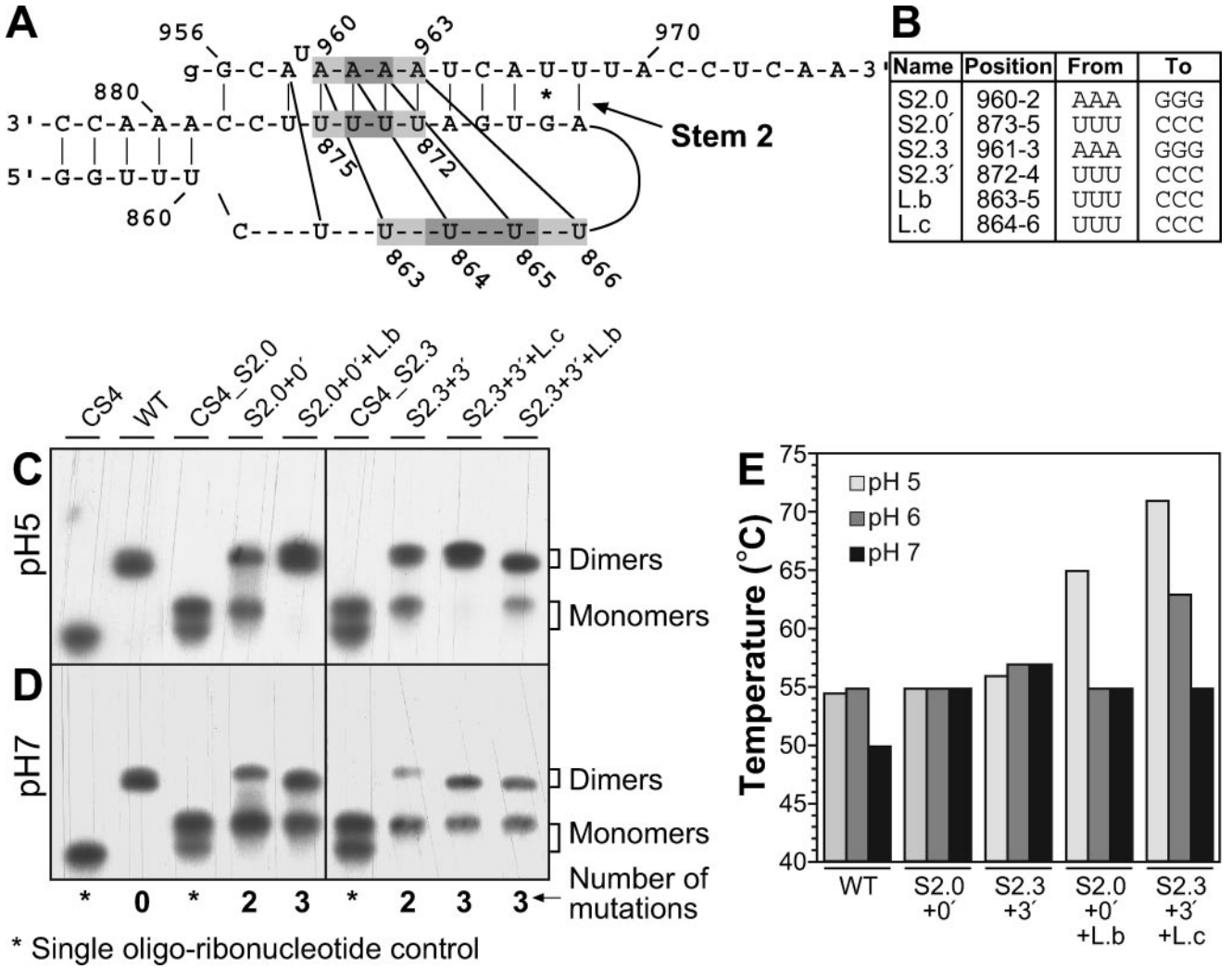

FIG. 6. pH-dependent dimer formation by oligoribonucleotides. (A and B) A schematic model of the *K. lactis* pseudoknot with five base triples (A), with the positions of the mutations (B) highlighted in gray. (C and D) Radioactively labeled CS4 and unlabeled CS3 (0.1 and 0.2 pmol, respectively) were analyzed as described in the legend to Fig. 3 and Materials and Methods. Identical gels were run simultaneously at pH 5 (C) and pH 7 (D). Single oligoribonucleotides are indicated by CS4 above and asterisks below the lanes. Lanes with mixtures of both CS3 and CS4 are indicated by the name (above) and number (below) of mutations introduced. (E) UV melting experiments were performed using various oligoribonucleotides at pH 5, 6, and 7. The T_m values were determined as described in Materials and Methods.

tions of the WT U-A · U and the mutant C-G · U triple helices is consistent with the relatively moderate effect of the corresponding mutation (S2.3+3′) on dimer formation (Fig. 3) and telomerase function (Fig. 2).

In summary, the triple-helix structure is consistent with several observations. First, double-transversion mutations in the triple-helical part of stem 2 (S2.2+2′ and S2.4+4′) failed to restore dimer formation in vitro (Fig. 3 and data not shown) and telomerase function in vivo (Fig. 2) (32). In contrast, double compensatory mutations in the double-helical part fully restored dimer formation (Fig. 3, S2.1+1′) and telomerase function (Fig. 1, S2.6+6′, and 1/1′ in reference 32). Second, single mutations in the CS3 loop completely abolished the dimer formation (Fig. 3, L.c) and telomerase function (Fig. 2, L.b, L.c, and L.d). The double-transversion mutations and the single mutations in the loop disrupted Hoogsteen hydrogen bonds and thus the triple-helix formation. Presumably, without the formation of the triple helix, the loop could not be accommodated anymore by the pseudoknot structure because it would clash with stem 2. Therefore, the interaction between CS3 and CS4 to form the pseudoknot structure was not possible in these mutants. Third, the transition double mutation S2.3+3′ had an intermediate effect, partially restoring the dimer formation (Fig. 3) and telomerase function (Fig. 2). Modeling studies revealed that this mutation could still retain a triple-helical structure composed of C-G · U base triples (Fig. 4B, D, and E), consistent with its intermediate effects on dimer formation and telomerase function.

Triple mutations. To test the triple-helix prediction, we combined three mutations, one in each strand of the triple helix (S2.3+3′+L.c and S2.0+0′+L.b) (Fig. 6A and B). In these mutants, the substituted cytosines in the third strand (L.b and L.c) must be protonated at their N3 positions to form C-G · C^+ triples. Therefore, these base triples depend on low

pH. Such triples (Fig. 4F) have been studied extensively for DNA (see, e.g., reference 23). For RNA, a single C-G · C^+ triple was observed in stem 2 of the frameshifting pseudoknot from the beet western yellow virus (26). This base triple contributed to the pseudoknot stabilization in a pH-dependent manner (21). In our case, while mutation L.c alone completely abolished dimer formation (Fig. 3C), the combined mutation S2.3+3′+L.c fully restored it at pH 5 but not at pH 7 (Table 2; compare Fig. 6C to D). Not only were the amounts of dimers formed reduced at pH 7, but their electrophoretic mobility also was slightly increased, suggesting that their structure was altered. In contrast, the formation of dimers by the WT sequences was not pH dependent, neither in the amount of dimers formed nor in their electrophoretic mobility. When introduced into *K. lactis* cells, the loop mutations abolished telomerase function in vivo (Fig. 2, L.b and L.c). Strikingly, adding the corresponding double mutations S2.0+0′ or S2.3+3′ to the loop mutations L.b or L.c, respectively, partially restored telomerase function, as revealed by the normal colony phenotypes, the mildly shortened telomeres (60 to 80% of the WT length), and the incorporation of BclI telomeric repeats (Fig. 2 and Table 2). Furthermore, growing the yeast at low temperature (16°C) fully restored normal telomere length in both double and triple mutants but not in the loop (L.c) mutant (Fig. 2F). The ability to suppress the phenotype by low growth temperature suggested that the double and triple mutations reduced the pseudoknot stability rather than significantly altering its structure. When the 3-nt substitution in the CS3 loop was shifted by one nucleotide towards stem 1 (from L.c to L.b), the triple mutation still supported dimer formation in vitro, albeit with somewhat reduced stability (Fig. 6C and D and Table 2, S2.3+3′+L.b). This mutation was expected to fix the third strand in a different register relative to the duplex, consistent with the alternative conformation of the pseudoknot (see above). A small but reproducible change in the dimer mobility was observed for this mutation (Fig. 6C), suggesting that the global structure of the pseudoknot was altered. Strikingly, when introduced into *K. lactis* cells, S2.3+3′+L.b and a similar mutation, S2.0+0′+L.a, abolished or severely impaired telomerase function (Fig. 2). We observed a 43% reduction in the level of TER in the S2.3+3′+L.b mutant (Table 2), which could have reduced telomerase activity. However, we observed a reduction of 90% in the level of TER in an unrelated mutant in another region, while it was still active and able to maintain stable telomeres, even if very short (not shown). In addition, the reduction of 40% in the level of TER in another unrelated mutant caused only slight shortening of telomeres (not shown). Therefore, although the reduction in the level of TER may exacerbate the phenotype, it is clearly not sufficient to account for the complete telomerase deficiency of the S2.3+3′+L.b mutant.

To study the sequences synthesized by the telomerase triple mutants, we cloned and sequenced at least 10 individual telomeres from each of the strains by using a ligation-mediated PCR method. Interestingly, we found truncated repeats in the S2.3+3′+L.c and S2.0+0′+L.a telomeres (one example for each mutant is shown in Fig. 7). Such truncated repeats were previously observed in the S2.3+3′ mutant, as well as in template boundary mutants (32), but never in any other telomere clones from wild-type or mutant strains. We did not find such

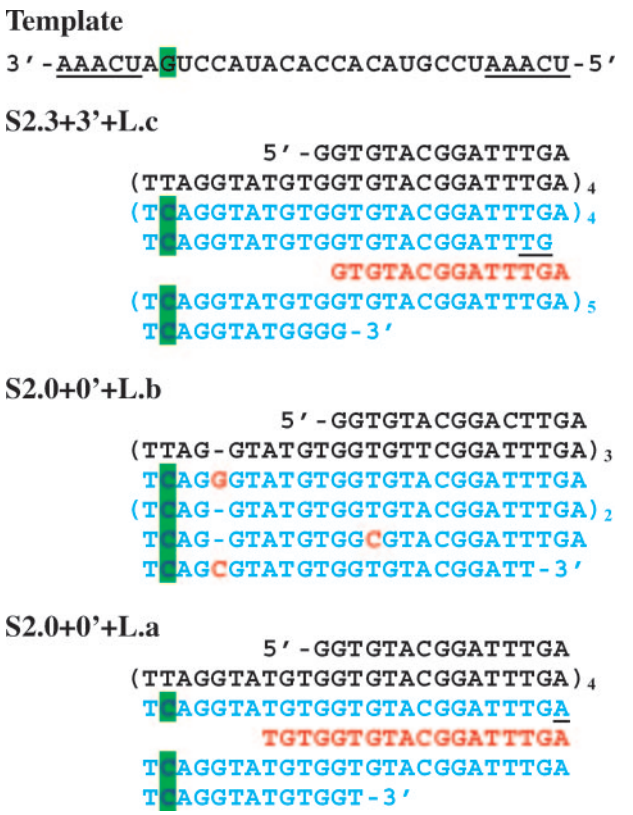

FIG. 7. Incorporation of truncated and mutated repeats onto telomeres in vivo. Shown are examples of cloned telomere sequences from the S2.3+3′+L.c, S2.0+0′+Lb, and S2.0+0′+La mutant strains at their sixth passage after introducing the mutant *ter* gene. The telomeric repeats are aligned to the template sequence above. Underlined are the repeated sequence at the beginning and the end of the template. Underlined in the S2.3+3′+L.c and S2.0+0′+La telomeres are nucleotides used for base-pairing and initiating the synthesis of truncated repeats from the middle of the template. The telomerase template and wild-type telomeric repeats are shown in black; BclI repeats synthesized by the mutant telomerase, in blue; truncated repeats and misincorporated nucleotides, in red. The BclI mutations are highlighted in green.

truncated repeats in the S2.0+0′+L.b telomeres, but instead they contained mutations in the nascent portions of the telomere (Fig. 7). Although at present we do not have a mechanistic interpretation of these results, they nevertheless show that the structural details of the pseudoknot are crucial for telomerase function. The triple mutations not only reduced telomerase activity and telomere length but also altered the nature of telomere synthesis, indicating that the pseudoknot is intimately involved in telomerase action.

We tested additional combinations of double mutations, and all of them abolished telomerase function, further confirming that the pseudoknot structure is essential (Fig. 2 and Table 1, S2.3′+L.c, S2.3+L.c, S2.0′+L.b, and S2.0′+L.a). Altogether, in vitro and in vivo analyses of various disruptive mutations and compensatory mutations forming C-G · U or C-G · C^+ base triples confirmed the triple-helix model and indicated that not only the stability but also the precise structure of the pseudoknot is essential for telomerase function.

Thermal melting. We next monitored the thermal denaturation of oligoribonucleotides in solution by following the absorption at 260 nm along a temperature gradient. A cooperative transition was observed for the mixture of WT CS3 and CS4 sequences, presumably indicating the melting of the CS3-CS4 dimers. No such a transition was observed for each sequence alone (not shown). The T_m of the WT dimer was only slightly affected by pH (50 to 55°C at pH 7 to 5) (Fig. 6E and Table 2). Similar pH-independent T_m values of 55°C and 56 to 57°C were observed for the double mutants S2.0+0′ and S2.3+3′, respectively, yet these mutations only partially restored dimer formation as observed by native PAGE (Fig. 6D and E) and telomerase function in vivo (Fig. 2C and D). This suggested that although they have similar midpoints of dissociation (T_m values), mutant constructs might be less stable than the WT at room temperature. Mechanical forces may enhance the dissociation of the mutant dimers during prolonged gel electrophoresis under such circumstances, as has been observed for kissing hairpin complexes of the human immunodeficiency virus type 1 dimerization initiation site (27). Adding the third mutation significantly increased the stability of the structure in a pH-dependent manner (Fig. 6 and Table 2). At pH 7, the triple mutations S2.0+0′+L.b and S2.3+3′+L.c had T_m values similar to those of the double mutations (55°C). However, these values dramatically increased to 65°C and 71°C, respectively, at pH 5, consistent with the protonation of cytosines and the formation of C-G · C^+ triples. This was consistent with the efficient dimer formation of the triple mutants at pH 5, as observed by native PAGE. However, these T_m values were significantly higher than that of the WT. In addition, the corresponding triple mutants only partially restored telomerase function in vivo (Fig. 2). One can think of several possible explanations. If the intranuclear pH was higher than the pK_a of the substituted cytosines in the CS3 loop, these cytosines would not be protonated and would not form triples. Indeed, at pH 7 these mutants had T_ms similar to those of the double C-G · U mutants and behaved similarly on native PAGE, except for the increased mobility of the C-G · C mutants at pH 7. They also had similar telomerase activity in vivo. If, on the other hand, the intranuclear pH is low enough to allow protonation of the C residues, the inability to fully restore telomerase function may indicate the overstabilization of the structure, supporting the conformational switch model (6). However, the suppression of the telomere phenotype by growing the triple mutant at low temperature (16°C) argues against this possibility. Finally, the internal pH may be close enough to the pK_a values to allow partial protonation and partial formation of the correct structure.

Conservation of the triple-helix structure between *K. lactis* and human. During the course of our research, an independent work has been published, reporting on the nuclear magnetic resonance solution structure of the human telomerase pseudoknot (29). Remarkably, this structure revealed features similar to the 3D model of the *K. lactis* pseudoknot reported here, most importantly, the presence of a triple helix within stem 2. At the same time, there are many significant differences between the two structures. There are five consecutive U-A · U triples in the *K. lactis* pseudoknot and only three in the human pseudoknot. Stem 2 is longer (12 bp) and the loop is shorter (6 nt) in *K. lactis* than in human (9 bp and 8 nt, respectively). Therefore, the loop in the *K. lactis* pseudoknot is much more constrained and structured. The details of the junction between stems 1 and 2 are also quite different. In *K. lactis*, stem 2 ends with a Watson-Crick G · C pair, there is a triple of unpaired cytosines just next to it, and the helical twist angle between stems 1 and 2 is 56°. In human, there is a non-Watson-Crick A · U pair at the junction of the two stems, and the twist angle is 75 to 80°. The human structure was solved for a mutant RNA construct in which a bulged nucleotide in stem 2 (U177) was deleted. Its deletion was suggested previously to reduce human telomerase activity (to 10% of the WT activity) by stabilizing the pseudoknot structure and impairing the function of the pseudoknot as a molecular switch (6). However, the reduction in telomerase activity of the U177 deletion mutant may also result from an alteration of the pseudoknot structure, rather than from the increased pseudoknot stability. As described above for the *K. lactis* pseudoknot, one nucleotide shift in the register of the triple helix, presumably affecting the junction between stem 1 and 2, completely abolished telomerase function (Fig. 2, compare S2.3+3′+L.c to S2.3+3′+L.b and S2.0+0′+L.b to S2.0+0′+L.a). These results demonstrated how crucial are at least some aspects of the pseudoknot structure. In *K. lactis*, the length of stem 2 (12 bp) and the increased stability due to the triple-helix formation argue against the involvement of stem 2 in a conformational switch. However, a shift between different registers of the triple helix is theoretically possible. If such a switch was required, fixing the structure in either conformation would impair telomerase function. Such a model can explain why the triple mutations that preserved a stable triple helix in vitro failed to fully restore telomerase function in vivo. However, without experimental evidence this remains a speculation.

Conclusion. We carried out a detailed analysis of the pseudoknot structure in *K. lactis* telomerase RNA. The successful integration of phylogenetic, molecular, and genetic analyses with molecular modeling yielded a 3D structure, which in turn was confirmed by additional mutational analyses in vitro and in vivo. Although the calculated model is not a high-resolution structure, its accuracy, predictive power, and in vivo relevance were demonstrated. Computer modeling is not routinely used to predict 3D structures of complex RNA molecules. Nevertheless, its usefulness is clear. One example is a computer prediction of the 3D architecture of group I catalytic introns (19), two decades before their crystal structures were solved (reviewed in reference 35). The success in developing a 3D model for the *K. lactis* pseudoknot was largely due to the highly constrained nature of this structural element: only 4 out of 41 residues are not part of base pairs or triples (Fig. 5B). This model is also supported by the conservation found in the pseudoknot within TER sequences of the "*Kluyveromyces marxianus*" cluster of species (Fig. 8). Furthermore, it is consistent with experiments with *S. cerevisiae* (3, 10, 13) suggesting that a similar U-A · U triple helix also forms in TLC1. While the homology of stem 2, including the triple helix, is apparent for *K. lactis*, *S. cerevisiae*, and human sequences, there are possible alternative arrangements for stem 1 in *S. cerevisiae*. In addition, while stem 2 and the junction between stems 1 and 2 are critical for telomerase function, mutations in the predicted stem 1 seem to be less detrimental (Fig. 1). Deletions in the

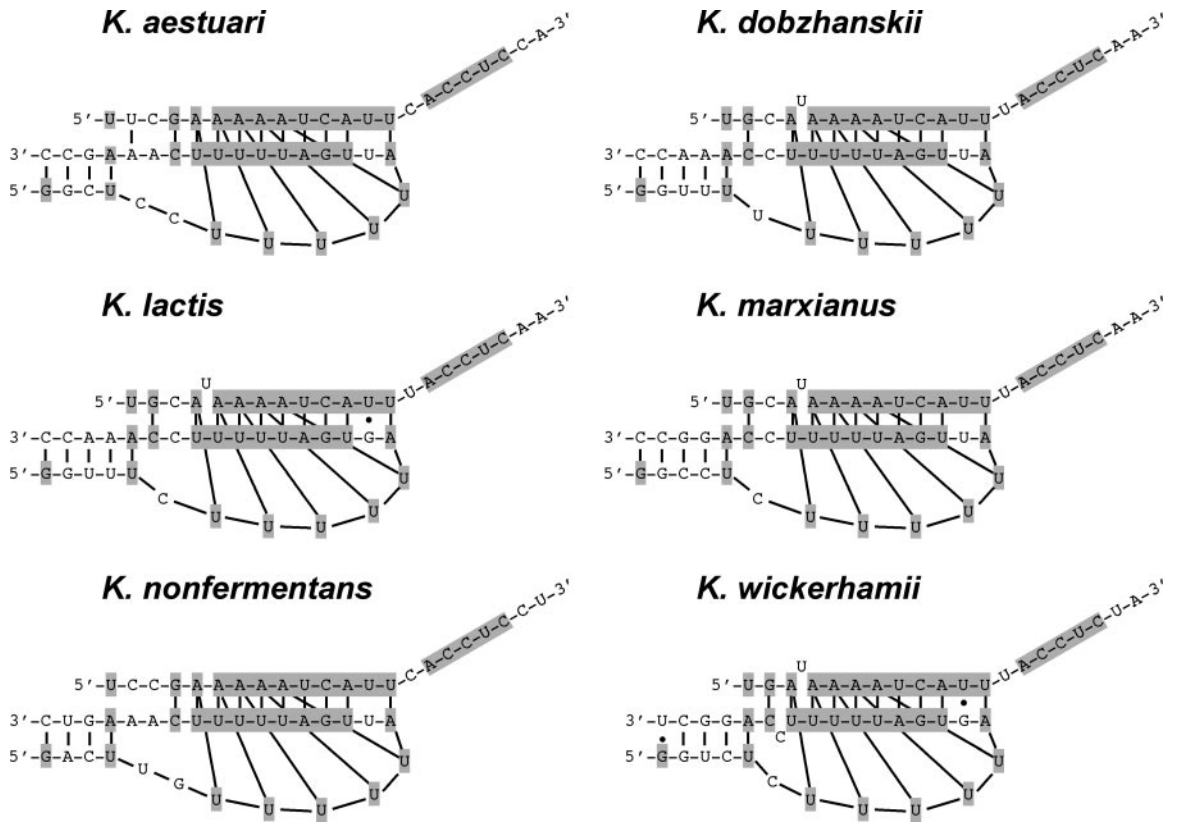

FIG. 8. Conservation of the triple-helix pseudoknot in the "*Kluyveromyces marxianus*" cluster of species. Pseudoknot models are shown for the *TER* sequences of six *Kluyveromyces* species (32). Conserved residues are highlighted in gray. Hoogsteen interactions are indicated as tilted lines.

sequences corresponding to stem 1 in *S. cerevisiae* had little or no effect on telomerase function (3, 13). Altogether, these observations suggested that stem 2 with the triple helix is the most crucial and conserved part of this element. In some species it may be sufficient to provide the essential function of this domain. Strikingly, the much smaller ciliate pseudoknot can partially substitute for the *S. cerevisiae* and human domains (3, 16), suggesting the presence of this conserved functional element in all telomerases.

A major-groove triple helix was proposed in 1957 for the synthetic polymer poly(rU)-poly(rA) · poly(rU) (8). Those authors suggested that "this three-stranded structure may have significance as a prototype for a biologically important three-stranded complex." Isolated base triples have been found in RNA structures. However, to the best of our knowledge, the telomerase RNA pseudoknot is the first example found in a native RNA molecule of consecutive U-A · U triples forming a major-groove triple helix. Furthermore, it represents the first structural element conserved between the otherwise highly divergent yeast and human telomerase RNAs.

In the telomerase catalytic core model, the pseudoknot is juxtaposed to the telomerase template by the core-enclosing helix (13). Interestingly, cloned telomeres from the triple-helix mutants revealed defects in processivity and fidelity of the enzyme (Fig. 7) (32). These aberrations in telomere synthesis suggested that the pseudoknot is intimately involved in the telomerase reaction. Experiments with *S. cerevisiae* indicated that pseudoknot sequences are important for Est2 binding (3, 13, 15), but no indication for a direct interaction with the pseudoknot sequences was found. Since this unusual triple-helical pseudoknot is conserved between human, yeast, and possibly also ciliate telomerases but has not yet been found elsewhere in nature, we propose that it contributes an essential function, conserved and unique to the telomerase ribonucleoprotein, which is yet to be uncovered.

ACKNOWLEDGMENTS

This work was supported by United States-Israel Binational Science Foundation grant 2001065 to Y.T. and N.B.U. and by Israel Science Foundation Grant 676/02 to Y.T.

We thank Tom Goddard, Tom James, Elly Ordan, Debbie Shalev, Joseph Shlomai, Ruth Sperling, and Eric Westhof for critical reading of the manuscript and for stimulating conversations. N.B.U. is indebted to Tom James for his encouragement and continuing support.

REFERENCES

1. **Ban, N., P. Nissen, J. Hansen, P. B. Moore, and T. A. Steitz.** 2000. The complete atomic structure of the large ribosomal subunit at 2.4 A resolution. Science **289:**905–920.
2. **Cech, T. R.** 2004. Beginning to understand the end of the chromosome. Cell **116:**273–279.
3. **Chappell, A. S., and V. Lundblad.** 2004. Structural elements required for association of the *Saccharomyces cerevisiae* telomerase RNA with the Est2 reverse transcriptase. Mol. Cell. Biol. **24:**7720–7736.
4. **Chen, J. L., M. A. Blasco, and C. W. Greider.** 2000. Secondary structure of vertebrate telomerase RNA. Cell **100:**503–514.
5. **Church, G. M., and W. Gilbert.** 1984. Genomic sequencing. Proc. Natl. Acad. Sci. USA **81:**1991–1995.
6. **Comolli, L. R., I. Smirnov, L. Xu, E. H. Blackburn, and T. L. James.** 2002. A molecular switch underlies a human telomerase disease. Proc. Natl. Acad. Sci. USA **99:**16998–17003.

7. **Dandjinou, A. T., N. Levesque, S. Larose, J. F. Lucier, S. Abou Elela, and R. J. Wellinger.** 2004. A phylogenetically based secondary structure for the yeast telomerase RNA. Curr. Biol. **14:**1148–1158.
8. **Felsenfeld, G., D. R. Davies, and A. Rich.** 1957. Formation of a three-stranded polynucleotide molecule. J. Am. Chem. Soc. **79:**2023–2024.
9. **Ferrin, T. E., C. C. Huang, L. E. Jarvis, and R. Langridge.** 1988. The MIDAS display system. J. Mol. Graph **6:**13–27.
10. **Forstemann, K., and J. Lingner.** 2005. Telomerase limits the extent of base pairing between template RNA and telomeric DNA. EMBO Rep. **6:**361–366.
11. **Frank-Kamenetskii, M. D., and S. M. Mirkin.** 1995. Triplex DNA structures. Annu. Rev. Biochem. **64:**65–95.
12. **Giedroc, D. P., C. A. Theimer, and P. L. Nixon.** 2000. Structure, stability and function of RNA pseudoknots involved in stimulating ribosomal frameshifting. J. Mol. Biol. **298:**167–185.
13. **Lin, J., H. Ly, A. Hussain, M. Abraham, S. Pearl, Y. Tzfati, T. G. Parslow, and E. H. Blackburn.** 2004. A universal telomerase RNA core structure includes structured motifs required for binding the telomerase reverse transcriptase protein. Proc. Natl. Acad. Sci. USA **101:**14713–14718.
14. **Lingner, J., L. L. Hendrick, and T. R. Cech.** 1994. Telomerase RNAs of different ciliates have a common secondary structure and a permuted template. Genes Dev. **8:**1984–1998.
15. **Livengood, A. J., A. J. Zaug, and T. R. Cech.** 2002. Essential regions of *Saccharomyces cerevisiae* telomerase RNA: separate elements for Est1p and Est2p interaction. Mol. Cell. Biol. **22:**2366–2374.
16. **Marie-Egyptienne, D. T., M. A. Cerone, J. A. Londono-Vallejo, and C. Autexier.** 2005. A human-Tetrahymena pseudoknot chimeric telomerase RNA reconstitutes a nonprocessive enzyme in vitro that is defective in telomere elongation. Nucleic Acids Res. **33:**5446–5457.
17. **McEachern, M. J., and E. H. Blackburn.** 1996. Cap-prevented recombination between terminal telomeric repeat arrays (telomere CPR) maintains telomeres in Kluyveromyces lactis lacking telomerase. Genes Dev. **10:**1822–1834.
18. **McEachern, M. J., and J. B. Hicks.** 1993. Unusually large telomeric repeats in the yeast *Candida albicans*. Mol. Cell. Biol. **13:**551–560.
19. **Michel, F., and E. Westhof.** 1990. Modelling of the three-dimensional architecture of group I catalytic introns based on comparative sequence analysis. J. Mol. Biol. **216:**585–610.
20. **Mozdy, A. D., and T. R. Cech.** 2006. Low abundance of telomerase in yeast: implications for telomerase haploinsufficiency. RNA **12:**1721–1737.
21. **Nixon, P. L., and D. P. Giedroc.** 2000. Energetics of a strongly pH dependent RNA tertiary structure in a frameshifting pseudoknot. J. Mol. Biol. **296:**659–671.
22. **Poltev, V. I., and N. V. Shulyupina.** 1986. Simulation of interactions between nucleic acid bases by refined atom-atom potential functions. J. Biomol. Struct. Dyn. **3:**739–765.
23. **Radhakrishnan, I., and D. J. Patel.** 1994. Solution structure of a pyrimidine.purine.pyrimidine DNA triplex containing T.AT, C+.GC and G.TA triples. Structure **2:**17–32.
24. **Romero, D. P., and E. H. Blackburn.** 1991. A conserved secondary structure for telomerase RNA. Cell **67:**343–353.
25. **Roy, J., T. B. Fulton, and E. H. Blackburn.** 1998. Specific telomerase RNA residues distant from the template are essential for telomerase function. Genes Dev. **12:**3286–3300.
26. **Su, L., L. Chen, M. Egli, J. M. Berger, and A. Rich.** 1999. Minor groove RNA triplex in the crystal structure of a ribosomal frameshifting viral pseudoknot. Nat. Struct. Biol. **6:**285–292.
27. **Takahashi, K. I., S. Baba, P. Chattopadhyay, Y. Koyanagi, N. Yamamoto, H. Takaku, and G. Kawai.** 2000. Structural requirement for the two-step dimerization of human immunodeficiency virus type 1 genome. RNA **6:**96–102.
28. **ten Dam, E., A. van Belkum, and K. Pleij.** 1991. A conserved pseudoknot in telomerase RNA. Nucleic Acids Res. **19:**6951.
29. **Theimer, C. A., C. A. Blois, and J. Feigon.** 2005. Structure of the human telomerase RNA pseudoknot reveals conserved tertiary interactions essential for function. Mol. Cell **17:**671–682.
30. **Theimer, C. A., and J. Feigon.** 2006. Structure and function of telomerase RNA. Curr. Opin. Struct. Biol. **16:**307–318.
31. **Tzfati, Y., T. B. Fulton, J. Roy, and E. H. Blackburn.** 2000. Template boundary in a yeast telomerase specified by RNA structure. Science **288:**863–867.
32. **Tzfati, Y., Z. Knight, J. Roy, and E. H. Blackburn.** 2003. A novel pseudoknot element is essential for the action of a yeast telomerase. Genes Dev. **17:**1779–1788.
33. **Ulyanov, N. B., K. D. Bishop, V. I. Ivanov, and T. L. James.** 1994. Tertiary base pair interactions in slipped loop-DNA: an NMR and model building study. Nucleic Acids Res. **22:**4242–4249.
34. **Ulyanov, N. B., and T. L. James.** 1995. Statistical analysis of DNA duplex structural features. Methods Enzymol. **261:**90–120.
35. **Vicens, Q., and T. R. Cech.** 2006. Atomic level architecture of group I introns revealed. Trends Biochem. Sci. **31:**41–51.
36. **Westhof, E., and L. Jaeger.** 1992. RNA pseudoknots. Curr. Opin. Struct. Biol. **2:**327–333.
37. **Zappulla, D. C., and T. R. Cech.** 2004. Yeast telomerase RNA: a flexible scaffold for protein subunits. Proc. Natl. Acad. Sci. USA **101:**10024–10029.
38. **Zhurkin, V. B., Y. P. Lysov, and V. I. Ivanov.** 1978. Different families of double-stranded conformations of DNA as revealed by computer calculations. Biopolymers **17:**377–412.
39. **Zhurkin, V. B., V. I. Poltev, and V. L. Florentiev.** 1980. Atom-atomic potential functions for conformational calculations of nucleic acids. Molek. Biol. **14:**882–895.
40. **Zhurkin, V. B., N. B. Ulyanov, A. A. Gorin, and R. L. Jernigan.** 1991. Static and statistical bending of DNA evaluated by Monte Carlo simulations. Proc. Natl. Acad. Sci. USA **88:**7046–7050.